JMEPEG (2010) 19:1133–1142
DOI: 10.1007/s11665-010-9597-1

1059-9495/$19.00

Study of Glazes and Their Effects on Properties of Triaxial Electrical Porcelains from Ugandan Minerals

Peter W. Olupot, Stefan Jonsson, and Joseph K. Byaruhanga

(Submitted December 1, 2009; Accepted: 30 December 2009)

Kaolin, ball clay, feldspar, and sand were collected from deposits in Uganda, milled and sieved to particle sizes of 45, 45, 53, and 25 µm, respectively. Three porcelain bodies and five glazes were formulated from them. The glazes were applied on porcelain specimens and subsequently evaluated for their effects on properties of porcelain samples. The formulated specimens were investigated using dilatometry, Steger test, FEG-SEM, XRD, 4-point bending, dielectric strength, and fracture toughness tests. A porcelain specimen consisting of 68% SiO_2, 19% Al_2O_3, 4.7% K_2O, and a glaze RO:0.57Al_2O_3:4.86SiO_2 exhibited MOR of 105 MPa with Weibull modulus of 5.6 and a dielectric strength of 18 kV/mm upon firing at a heating rate of 6 °C/min to 1250 °C and holding for 2 h. The microstructure of the high-strength specimen exhibited round mullite needles, quartz, and glass. Holding samples for 2 h at peak temperature resulted in a 22% increase in MOR compared to 1 h holding. Glazing further improved strength by 67% for the best sample. Compressive stresses in glaze contributed to the strengthening effect. The dielectric and mechanical strength values obtained qualify the formulated sample for application in electrical insulation.

Keywords advanced characterization, chemical analysis, electron microscopy, mechanical testing, structural ceramics

1. Introduction

In porcelain production, glazing is one of the most important steps from both the technological and esthetic points of view. Glazes can either be raw or fritted. If the glaze does not contain water soluble constituents then, for such, a raw glaze is more advantageous than a fritted one due to being matured in a short time with lower cost (Ref 1). The glaze-body interactions which take place during glost firing depend on several variables. These include, composition of the body and the glaze, the thickness of the glaze layer, the peak of the glost firing temperature and soak time, processing route (once fired or twice fired), whether or not the glaze is fritted and to what extent, the viscosity of the molten glaze, and the mutual solubility of the body and glaze components. These interactions during glost firing are of significance since they determine the physical, chemical, and mechanical properties of the as-fired glaze such as craze resistance, strength, abrasion properties, chemical resistance, esthetic appearance, and maturing behavior of the glaze (Ref 2). Because of these interactions, the same glaze fired on different bodies can give quite different surface qualities.

In relation to mechanical strength, porcelain tends to exhibit high values when the coefficient of thermal expansion of the interaction layer is intermediate between those of the glaze and the body. This also prevents crazing defects, especially where the thermal expansion coefficient of the glaze is close to that of the body (Ref 3). A low value of coefficient of thermal expansion of the glaze causes development of compressive stresses in the glaze layer. This state of stress retards crack propagation, hence the strength of the system is enhanced. Glazing further influences the strength of ceramic bodies through: formation of an even surface which reduces the number of notch points; formation of an intermediate layer with a composition affecting the stress distribution in the system which, in favorable situations enhances strength (Ref 4).

The specification and presentation of glazes is commercially done using the Seger formula. In a Seger formula, the oxides present are arranged in three columns: basic oxides, which are monovalent (R_2O), and divalent (RO) oxides on the left; intermediate or trivalent (R_2O_3) oxides, which have both basic and acidic properties, in the center; and acidic oxides, which are tetravalent (RO_2) or pentavalent (R_2O_5), on the right. R is the general symbol for the metallic atom and O represents oxygen. The sum of the first column is brought to one. For porcelain fired in cones 7-10, approximate glaze compositions will be RO:0.4-0.8Al_2O_3:3.0-5.0SiO_2. The ratio of silica to alumina is held in the range of 7:1 to 10:1. Ingredients with plate-like structures (kaolins) are included in the recipes in limited amounts because, too little will result in inadequate suspension and settling out of the oxides, whereas excessive additions will induce crawling defects caused by drying cracks. Typically recommended amount for kaolin is 8-10% (Ref 5).

In this work, glazes were formulated from materials sourced from deposits in Uganda. The best matching glaze was applied on three porcelain insulator bodies previously studied by the present authors (Ref 6), also formulated from materials sourced from Ugandan deposits. Subsequent specimens were characterized for mechanical and dielectric properties. Glazing and soaking the specimens at 1250 °C for 2 h was found to improve the properties, compared to 1 h soak.

Peter W. Olupot and **Stefan Jonsson**, Department of Material Science and Engineering, Royal Institute of Technology (KTH), SE-100 44 Stockholm, Sweden; and **Joseph K. Byaruhanga**, Department of Mechanical Engineering, Makerere University, P.O. Box 7062, Kampala, Uganda. Contact e-mail: polupot@tech.mak.ac.ug.

2. Minerals and Sample Preparations

2.1 Deposits

The raw minerals used in the present investigation were taken from different deposits in Uganda. Kaolin and feldspar were taken from the Mutaka deposit, ball clay from Mukono and quartz sand from Lido beach, Entebbe on the shores of Lake Victoria. The location and characteristics of these deposits have previously been described by Olupot et al. (Ref 7) and Kirabira et al. (Ref 8).

2.2 Mineral Processing

Representative samples of about two tonnes were collected from each deposit and processed for use in the present study. Each mineral was separately wet-milled, run over a magnetic iron separating tray to remove iron contaminations and sieved through aperture sizes of 53 μm for feldspar, 45 μm for kaolin and ball clay, and 25 μm for sand. The aperture sizes were selected on the basis of cited literature on improvement of porcelain strength (Ref 9-11). The sieved minerals were dried in air, except for ball clay which was used as slip with a dry content calculated using Brogniart's formula (Ref 12).

The obtained minerals were used as starting materials for preparation of various samples, as will be described in the subsequent paragraphs.

2.3 Formulation of Porcelains

Three porcelains, denoted B, D, and E, given in Table 1, were formulated using results from previous research on unglazed porcelains by the authors (Ref 6). For each porcelain composition, a slurry mix with the proportions indicated in Table 1, was prepared from the processed minerals, and milled for 3 h in a ball mill using a quartz grinding medium to ensure homogeneous mixing. The slips were dried at room temperature to form pastes of sufficient plasticity for extrusion through a de-airing pugmill, producing cylindrical specimens of 15 mm in diameter. To avoid mixing of the pastes, the ball mill and extruder were washed and cleaned after each batch. The produced cylinders were dried in air at room temperature and cut to 80 mm of length. Then, depending on the final experimental test, the dried bars were prepared differently, as will be explained below.

Table 1 Compositions of porcelains and glazes (wt.%)

Sample	B	D	E	G1	G2	G3	G4	G5
SiO_2	68.00	67.57	67.26	61.97	62.80	63.20	64.46	64.56
Al_2O_3	19.16	19.77	20.22	14.00	13.33	12.76	12.18	11.61
CaO	0.83	0.86	0.88	8.19	8.06	8.50	8.45	8.96
Fe_2O_3	0.98	1.10	1.15	0.27	0.25	0.25	0.25	0.25
K_2O	4.74	3.87	3.44	5.32	5.55	5.25	4.95	4.65
MgO	0.28	0.31	0.32	0.17	0.16	0.17	0.19	0.20
MnO	0.02	0.02	0.02	0.01	0.01	0.01	0.01	0.01
Na_2O	0.60	0.53	0.49	0.53	0.54	0.52	0.49	0.46
P_2O_5	0.07	0.08	0.08	0.04	0.04	0.04	0.04	0.04
TiO_2	0.35	0.43	0.45	0.04	0.04	0.04	0.04	0.04
LOI	5.31	5.97	6.33	9.07	8.66	8.95	8.84	9.17
Total	100.32	100.49	100.63	99.60	99.46	99.69	99.91	99.94

2.4 Formulation of Glazes

Five glazes, denoted G1 to G5 in Table 1, were prepared by mixing the dry, processed minerals described in section 2.2 and adding a low-melting oxide component, CaO, in the form of pure whiting ($CaCO_3$) supplied by Mineral Enterprises (Kenya). Approximately 1 kg of each glaze was prepared by crushing the mixture of powders using a mortar and pestle. Slips were prepared by adding water. Each slip was thoroughly stirred by hand to ensure a homogeneous mixture. Within the series of glazes, the SiO_2:Al_2O_3 ratio was deliberately chosen to increase monotonically from 7.52 for G1 to 9.53 for G5 in approximately even intervals of 0.5. Using the Seger formalism (Table 2) and a recommendation by Eppler and Obstler (Ref 5), the compositions were formulated to have Al_2O_3 and SiO_2 contents of 0.4-0.7 and 3-5, respectively.

2.5 Preparation of Specimens

2.5.1 Glaze Evaluations and Dielectric Strength Tests. The off-cuts of the extruded bars of porcelain E, described in section 2.3, were pulverized and dry-sieved through an aperture of 100 μm. The powder was pressed in a uniaxial press at 100 MPa to form discs of Ø50 mm and thickness 3 mm. The discs were further dried at 110 °C for 24 h and biscuit fired to 850 °C, using a heating rate of 6 °C/min up to 850 °C, 1 h soaking and a slow cooling rate by cooling in the furnace. The biscuit firing was introduced in order to give the specimens enough strength to ease handling. The discs were glazed by first dipping in water, then dipping in a glaze slip, and finally drying in air at room temperature. Ten discs were prepared for each glaze. The glazed specimens were all fired using a heating rate of 6 °C/min up to 1250 °C and cooled to 500 °C at a rate of 6 °C/min followed by furnace cooling. However, half of the discs were held at the peak temperature for 1 h and half of the discs were held there for 2 h in order to investigate the influence of soaking time on the appearance of the glazed surface.

2.5.2 Mechanical Testing and Microstructure Analyses. The dried bars, described in section 2.3, were further dried at 110 °C for 24 h and biscuit fired in the same way as described for the samples in section 2.5.1. Most samples were glazed by first dipping them in water and then dipping them in the G3 glaze slip, appearing as the optimum choice from firing tests of all glazes, described below. After drying, glazed and un-glazed specimens were fired using a heating rate of 6 °C/min up to a firing temperature of 1250 °C which was held for 1 h for un-glazed specimens and 2 h for glazed specimens, respectively. Another batch of unglazed specimens was fired and held at the top temperature for 2 h. In all cases, the samples were cooled to 500 °C at a rate of 6 °C/min followed by furnace cooling to room temperature. The longer firing time for

Table 2 Glaze composition according to Seger formalism

	G1	G2	G3	G4	G5
Na_2O	0.040	0.041	0.039	0.037	0.034
K_2O	0.268	0.279	0.260	0.249	0.228
CaO	0.692	0.680	0.702	0.714	0.737
Al_2O_3	0.650	0.617	0.573	0.558	0.519
SiO_2	4.890	4.943	4.862	5.063	4.945
SiO_2:Al_2O_3	7.5	8.0	8.5	9.1	9.5

the glazed specimens was needed in order to obtain smooth surfaces with high gloss, as will be explained later. The specimens prepared in this way were used for testing the bending strength, fracture toughness and for characterizing the microstructure and interface between glaze and bulk porcelain.

2.5.3 Dilatometer Tests. Some of the biscuit-fired porcelain specimens described in section 2.5.2 were cut into smaller pieces of approximately 15-25 mm length and tested in a dilatometer, as will be described below. In order to test the glazes, pellets of Ø16 mm by 6 mm height were produced by uniaxial dry-pressing of each glaze powder at 100 MPa. The produced cylinders were then biscuit fired in the same way as the porcelains, described in section 2.5.1, and tested in a dilatometer. Additionally, glaze pellets placed on a steel plate, were held on a refractory support and fired using a heating rate of 6 °C/min up to 1250 °C, soaked for 2 h and cooled to 500 °C at a rate of 6 °C/min followed by furnace cooling to room temperature. A fired specimen for glaze G3 was eventually shaped by polishing to make rectangular test piece of 4 by 6 by 13 mm to be tested in the dilatometer.

2.5.4 Steger Tests. In order to check the compatibility between bulk and glaze with respect to thermal expansion, samples for Steger tests were produced by slip casting using the processed minerals described in section 2.2. The bars were of standard size 318 mm long with a central glazed section of 100 mm length. The slip casted bars were biscuit fired using the same procedure as described in section 2.5.1. The portion for glazing was wetted and the glaze slurry was applied by dripping it onto the surface. The bars were dried in air at room temperature and fired at 6 °C/min up to1250 °C, soaked for 2 h and cooled to 500 °C at a rate of 6 °C/min followed by furnace cooling to room temperature.

3. Experimental Techniques

3.1 Gloss and Smoothness of Glazes

Based on previous work by Olupot et al. (Ref 13), the optimum firing temperature of the porcelains was fixed to 1250 °C using a holding time of 1 h at peak temperature. In order to evaluate the surface quality of each glaze after firing, glazed discs of porcelain E were fired at 1250 °C for 1 and 2 h, respectively, using a heating rate of 6 °C/min, cooled at 6 °C/min to 500 °C and let to cool to room temperature in the furnace, with the power switched off. For each glaze, five discs were fired for 1 h and five discs were fired for 2 h. The quality of the glazed surface was judged with respect to smoothness and gloss by the bare hands and naked eyes.

3.2 Dilatometry

The biscuit-fired specimens of all porcelains and glazes were examined with respect to length changes in a dilatometer (Netzsch Dil 402C, Germany) operated under Ar gas and a preload of 10 cN to hold the samples. In all cases the heating and cooling rates were set to 6 °C/min and the holding time at the peak temperature was set to 10 min. However, the porcelains were tested up to 1050 °C whereas the less refractory glazes were tested to 950 °C to avoid damaging the equipment due to sticking problems.

In order to evaluate the effect of firing temperature on the thermal length changes, pieces were broken and sectioned from unused, slip casted, biscuit-fired bars, described in section 2.5.4, of porcelain E and fired for 2 h at 1150, 1200, 1250, 1300, and 1350 °C, respectively. The samples were tested in the dilatometer up to 1050 °C using heating and cooling rates of 6 °C/min and a holding time of 10 min. The thermal length changes were evaluated on the cooling curves using the longest straight section of the curve, from 950 to 600 °C, i.e., from 100 °C below the peak temperature and down to a temperature slightly above the onset of the β-to-α inversion during cooling.

The recorded length change was divided by the original specimen length to yield relative values for the length changes.

3.3 Steger Test

In this test, samples were heated at a rate of 5 °C/min to 800 °C. At 800 °C the difference in bending compared to the initial "cold" value was measured in millimeters. Samples were not soaked, but the deflection was read directly at 800 °C. A positive deflection indicates compressive stress in the glaze, whereas a negative deflection indicates tensile stress in the glaze. This test was carried out for two samples (B and E) which exhibited the highest and lowest values of MOR, respectively, after glazing. The tests were performed at IFO Ceramics, Bromölla, Sweden.

3.4 Bending Strength

Un-glazed and glazed specimens were tested in a four-point bending fixture using a Testometric Universal Testing Machine (Model M500, Testometric Universal Testing Machine, UK). The crosshead speed was 1 mm/min and the spans between the upper and lower supports were 20 and 40 mm, respectively. A minimum of 13 specimens from each sample batch were tested for fracture strength. Using Weibull statistics, as described in earlier works (Ref 13), the modulus of rupture, MOR, was evaluated for a fracture probability of 0.632.

3.5 Fracture Toughness

The fracture toughness was evaluated on sectioned and polished specimens of the extruded and fired cylinders using an indentation technique. A minimum of five Vickers indentations, using a load of 1 kg and a hold time of 15 s, were made on the surface of each specimen. Immediately after the indentation, the diameters of the formed radial cracks were measured. Only well-defined indents, without chipping or cracks terminating at pores, were used in the evaluation. For each indentation, two measurements of the crack diameters were made and the average of 10 readings was put into the formula given by Evans and Wilshaw as cited by Baharav et al. (Ref 14).

$$K_{IC} = \frac{1}{\pi^{3/2} \tan \psi}\left(\frac{P}{D^{3/2}}\right) \quad \text{(Eq 1)}$$

where K_{IC} is the fracture toughness, ψ is the indenter cone half-angle (68°), P is the peak contact load, and D is the average value of the diameter of the radial cracks.

3.6 Dielectric Strength

The dielectric breakdown voltage was measured using an A.C. voltage with a frequency of 50 Hz applied through a transformer to the testing equipment, with the test specimen immersed in transformer oil. The voltage was gradually raised

(automatically) until the sample started conducting, causing a circuit breaker to trip.

3.7 Microstructure Characterization

The microstructures of the specimens were characterized using a light optical microscope (LOM) and a FEG-SEM instrument, LEO 1530 with a GEMINI column. Sectioned and polished specimens of the extruded and fired cylinders were used for the investigation. The specimens were first polished with a colloidal silica suspension (Struers OPS) for 10 min, cleaned, dried, and observed directly in the LOM and FEG-SEM instruments. Thereafter, the specimens were dipped in 40% concentrated hydrofluoric acid for 25 s, cleaned, dried, and studied again using FEG-SEM instruments. The cleaning procedures given to all specimens before examination included washing in water and alcohol before drying.

3.8 Phase Constitution

The phase assemblies in the fired porcelain samples were determined by x-ray diffraction using an X'pertPRO PANalytical x-ray diffractometer, PW 3050/60, with Ni-filtered K_α Cu-radiation generated by a 40 kV acceleration voltage and a 40 mA anode current. The specimens were pulverized and scanned from 10° to 75° 2θ operating the equipment at a 2θ scan-speed of 0.5 s/step and a 2θ step size of 0.02°. The x-ray peaks of the different phases were identified with the software of the equipment.

4. Results

4.1 Gloss and Smoothness of Glazes

When the glazed and fired discs of porcelain sample E were examined qualitatively, it became evident that all glazes produced smooth surfaces of high gloss. However, the G3 glaze appeared to show the best smoothness and appeared to be more uniformly distributed on the specimen surfaces, especially after 2 h firing at the peak temperature. Consequently, the G3 glaze was selected for further study using a 2 h soaking time at the firing temperature.

4.2 Dilatometry

Typical heating curves for the porcelains are given in Fig. 1 showing porcelain E as fired to 850 and 1250 °C, respectively. As seen, the heating curves are quite similar, except for the sintering, occurring for the biscuit-fired sample at high temperatures. Both curves show a small thermal expansion up to about 550 °C followed by a sudden expansion up to about 590 °C due to the α-to-β quartz inversion. Then, thermal contraction occurs due to β-quartz contraction and for the biscuit-fired sample sintering sets in at about 900-925 °C rendering a substantial shrinkage.

Biscuit-fired samples of porcelains B, D, and E showed a reduced sintering rate above 990 °C (as seen in Fig. 1 for porcelain E). As expected, this reduction cannot be seen in specimens sintered at 1150-1350 °C, as seen for porcelain E in the same figure.

The cooling curves for the porcelains are all very similar, and as a result, only data for porcelain E are reproduced. See Fig. 2, showing the cooling curves of porcelain E fired to 850 and 1150-1350 °C, respectively. The poorly consolidated

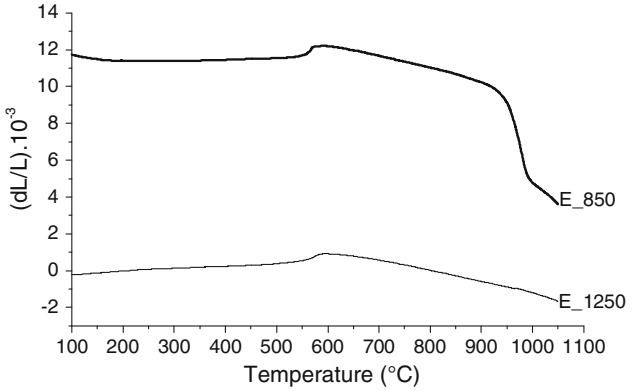

Fig. 1 Heating curves of porcelain E after firing at 850 and 1250 °C, respectively

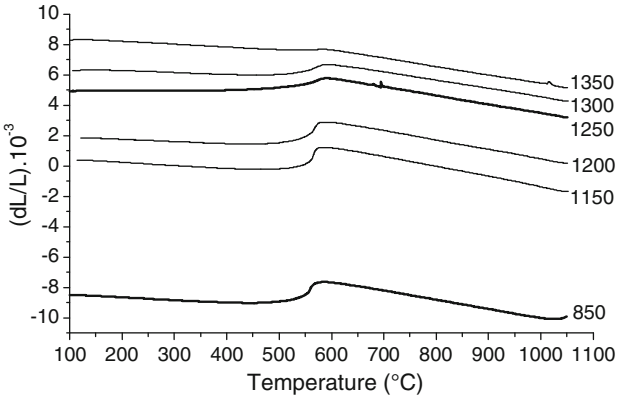

Fig. 2 Cooling curves of porcelain E after firing at different temperatures

biscuit-fired sample continues sintering in the very beginning of the cooling cycle, which can be seen as an initial shrinkage during cooling. Naturally, this behavior cannot be seen for the high-temperature sintered specimens. When sintering has stopped for the biscuit-fired sample, all specimens show an expansion with reduced temperature down to the β-to-α quartz inversion leading to a sudden contraction. Clearly from Fig. 2, this contraction is gradually reduced with sintering temperature resulting from the reduced amount of undissolved quartz. Below the inversion temperature of all specimens, except for the one sintered at 1250 °C, unexpectedly show an expansion with reduced temperature.

The heating and cooling curves for the glazes are all very similar and as a result, only the data for glaze G3 is reproduced in Fig. 3. First, a contraction occurs up to about 120 °C. Then, a thermal expansion follows which is suddenly interrupted by a contraction between about 300-440 °C. These two contractions are caused by the added $CaCO_3$ being confirmed by separate experiments on pure $CaCO_3$, not reported here. Naturally, these contractions cannot be seen for the porcelains, having no $CaCO_3$ added, as demonstrated by the heating curve in Fig. 1 for porcelain E. The rest of the heating curve is similar to the biscuit-fired E-porcelain of Fig. 1, i.e., a thermal expansion up to the α-to-β quartz inversion followed by thermal contraction and finally sintering. None of the glazes shows any sign of reduced sintering rate within the temperature range examined,

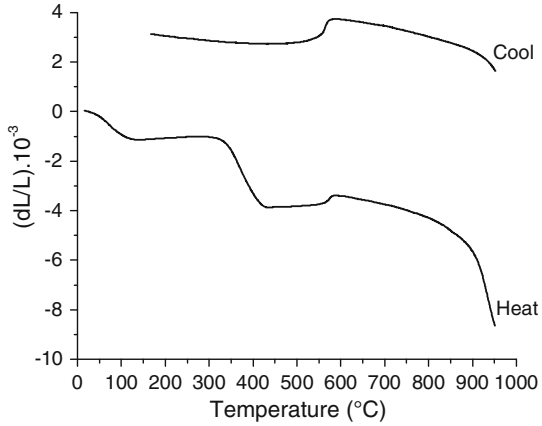

Fig. 3 Heating and cooling curves of glaze G3 after biscuit firing at 850 °C

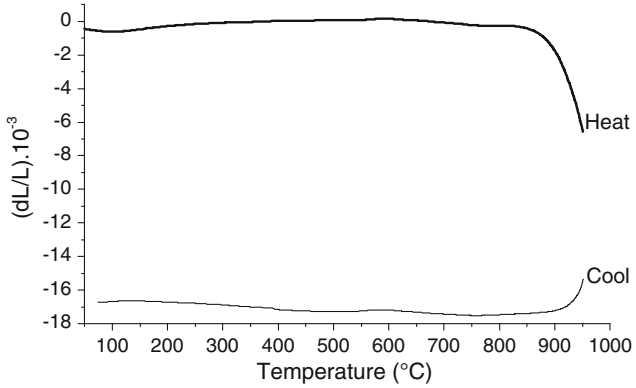

Fig. 4 Heating and cooling curves of glaze G3 after firing at 1250 °C

as observed for porcelains B and E, discussed in connection with Fig. 1.

The cooling curves for the glazes are very similar to each other and to the cooling curves of the porcelains. Compare Fig. 2 and 3. The β-to-α quartz inversion is quite clear in the glaze, probably because of the low sintering temperature and short soaking time used, quartz is not fully converted to glass. Indeed for the glazes fired to 1250 °C, there is no distinct quartz inversion point as shown in Fig. 4 for glaze G3. Apparently, the fired glaze starts to contract at about 850 °C, presumably because of shrinkage of pores formed at 1250 °C.

During sintering at the peak temperature, the biscuit-fired porcelains and glazes behave very differently. All biscuit-fired porcelains show a contraction during soaking whereas the biscuit-fired glazes initially show a contraction which is reverted to a clear expansion during the soaking. The expansion continues for a short period during cooling, as can be seen by the initial bend in the cooling curve in Fig. 3. The computed results of coefficients of thermal expansion are presented in Table 3 for the biscuit-fired glazes and the bulk specimens B, D, and E. In all porcelain samples, porcelain B has the highest magnitude of thermal coefficient of expansion.

The negative coefficients of thermal expansion for porcelain E, evaluated on the cooling curves for specimens fired and held at the different temperatures for 2 h are given in Fig. 5. The figure shows a trend of decreasing magnitude for the coefficient

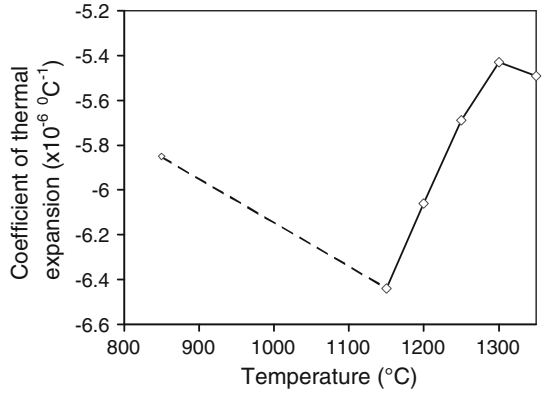

Fig. 5 Thermal expansion coefficient of porcelain E after 2 h firing at different temperatures. The point at 850 °C refers to biscuit firing

Table 3 Thermal expansion coefficients of glaze and porcelain samples fired to 850 °C

Glazes		Porcelain samples	
Glaze	$\alpha \times 10^{-7}$, °C^{-1}	Sample	$\alpha \times 10^{-7}$, °C^{-1}
G1	−41	B	−61.3
G2	−42.8	D	−54.0
G3	−48.2	E	−58.5
G4	−50.3		
G5	−46.8		

of thermal expansion as temperature increases for the temperature range of 1150 to 1300 °C, which is then abruptly broken by the 1350 °C sample. The trend is consistent with decreasing amount of undissolved quartz as firing temperature increases.

4.3 Bending Strength

The bending strengths of the three porcelain samples before and after glazing are given in Fig. 6. The unglazed samples were split into two batches; one batch was soaked at the top temperature of 1250 °C for 1 h while the other was soaked for 2 h. In all samples, holding at top temperature for 2 h resulted in increased modulus of rupture. There was a further increase upon glazing. For porcelain E, the increase in MOR upon glazing was much smaller than was for samples B and D. Sample B exhibited an increase in MOR of 22% upon increasing the soaking time from 1 to 2 h at the firing temperature. A further increase in strength of 67% was achieved upon glazing. The Weibull moduli, indicated by the slope of the regression lines of the samples, were almost identical for the glazed samples.

4.4 Fracture Toughness and Dielectric Strength

The effects of glazing and soaking at the peak temperature for 2 h on MOR, Weibull modulus, K_{IC} and dielectric strength are summarized in Fig. 7. Rising soaking time from 1 to 2 h is shown to increase the modulus of rupture in all the samples (Fig. 7a). The Weibull modulus, however, decreases (Fig. 7b). Upon glazing and soaking the samples for 2 h at the peak temperature, there is an improvement in both the modulus of rupture and Weibull modulus. Figure 7(c) also reveals a wide variation in K_{IC} for the samples upon glazing, i.e., prolonged

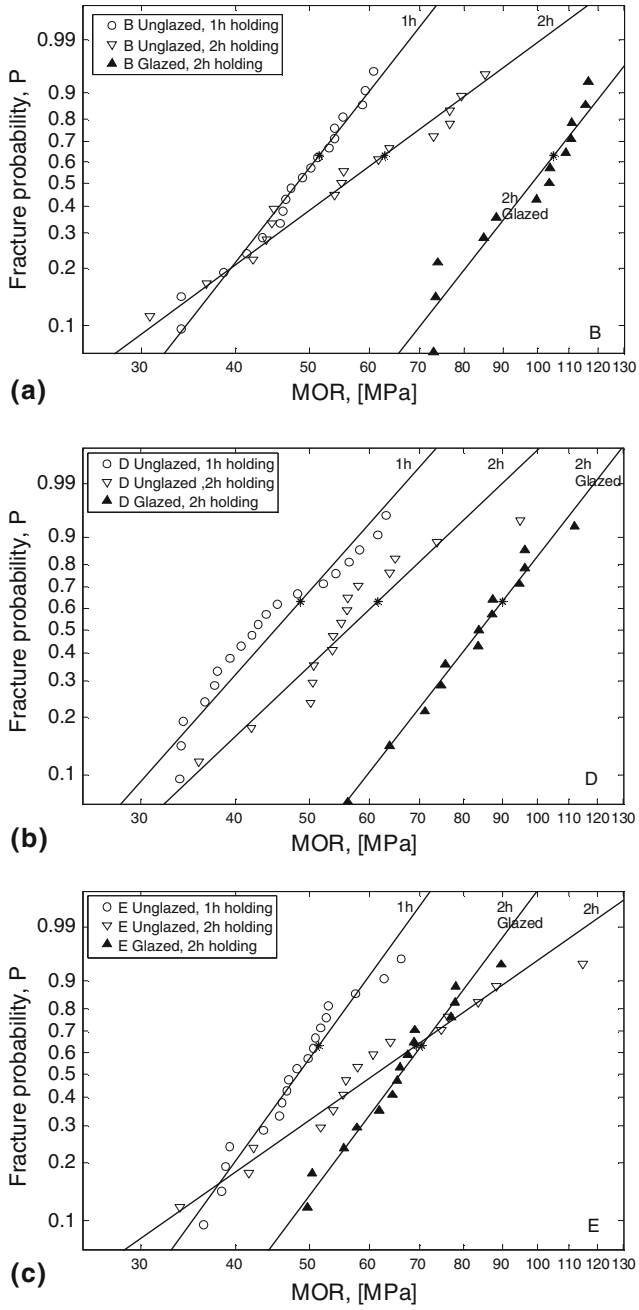

Fig. 6 Weibull plot of (a) sample B, (b) sample D, and (c) sample E, evaluated for 4-point bending load test. MOR at probability of 0.632 is indicated by "*"

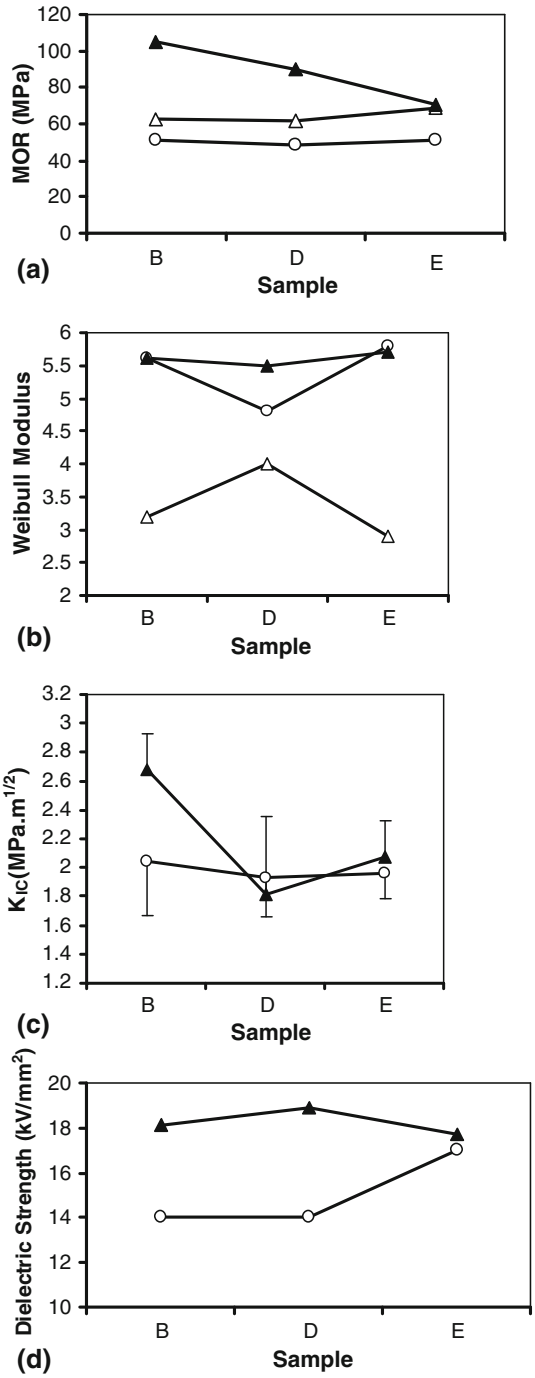

Fig. 7 (a) MOR, (b) Weibull modulus, (c) K_{IC}, and (d) dielectric strength of samples before and after glazing using glaze G3. Legends as in Fig. 6. For clarity, only positive error bars are shown for glazed samples in (c) while only negative error bars are shown for unglazed samples in the same figure

soaking as K_{IC} is tested in the interior of the specimen cross sections, unaffected by glazing. Sample B shows a significant improvement whereas samples E and D show minor improvement and reduction, respectively. The values for K_{IC} for sample D vary significantly as indicated by the high standard deviation represented by the error bar. Samples soaked for 1 h at peak temperature exhibit quite close magnitudes of K_{IC} whereas there is a scatter for the 2 h soaked specimens. This difference suggests a change in the structure of the sintered specimens as soaking time increases.

All the samples show an improvement in dielectric strength upon glazing. Samples B and D have significantly lower magnitudes of dielectric strength before glazing compared to sample E, the glazed samples, however, exhibited quite close values of dielectric strengths. This suggests that glazing plays a significant role in creating a uniform distribution of flaws in the samples and hence uniform dielectric properties.

4.5 Microstructure Characterization

The fired glaze thickness varies between 120 and 170 μm, followed by a transition zone between the glaze and the bulk

substrate, represented by a bright contrast in Fig. 8. The clarity of this zone diminishes in the order of samples B, D, and E, respectively. Light optical microscopy (LOM) reveals the presence of smooth round pores in the glaze at, or near, the interface between the glaze and the substrates in all samples, as indicated in Fig. 8. The scanning electron microscope (SEM) image in Fig. 8, for sample B shows the bottom of some sectioned pores. As seen, the interiors of the bubbles are smooth. After etching, on the other hand, a shell-like structure is seen inside the pores of sample E, Fig. 9, together with some shallow dimples on the etched surface. The smooth shallow dimples can be explained as the bottoms of etched pores. The shell-like structures, on the other hand, are more difficult to explain. EDS analysis reveals them to have a high concentration (about 68%) of *F*, probably introduced into the material during etching. It is thus tempting to suggest that they were formed during etching by some solution/recrystallization process. This is consistent with the fact that all LOM investigations could only show smooth, empty pores before etching. Interestingly, the shell-like structures could only be found in sample E after etching, which is further demonstrated in Fig. 10, for the low magnifications.

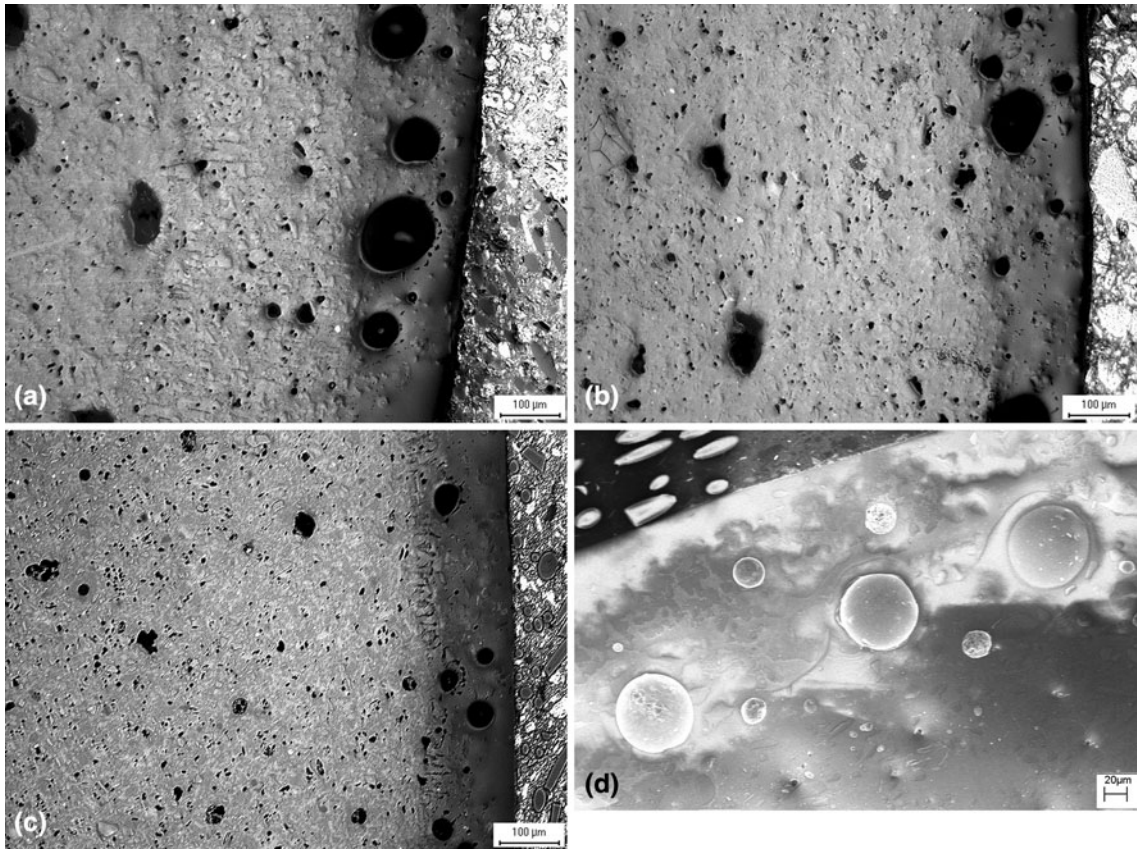

Fig. 8 LOM of glazed specimens of sample: (a) B, (b) D, (c) E, and (d) SEM image of sample B. Fired to 1250 °C and held at top temperature for 2 h. Not etched. For LOM images, the scale bar indicates 100 µm and for the SEM, it indicates 20 µm

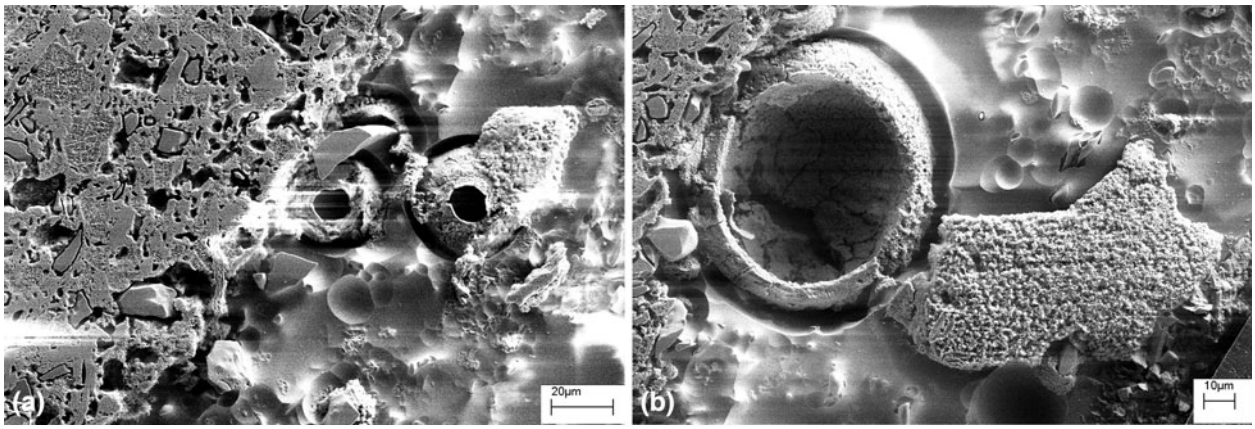

Fig. 9 SEM of sample E Fired to 1250 °C and held at top temperature for 2 h, polished and etched in 40%HF for 25 s

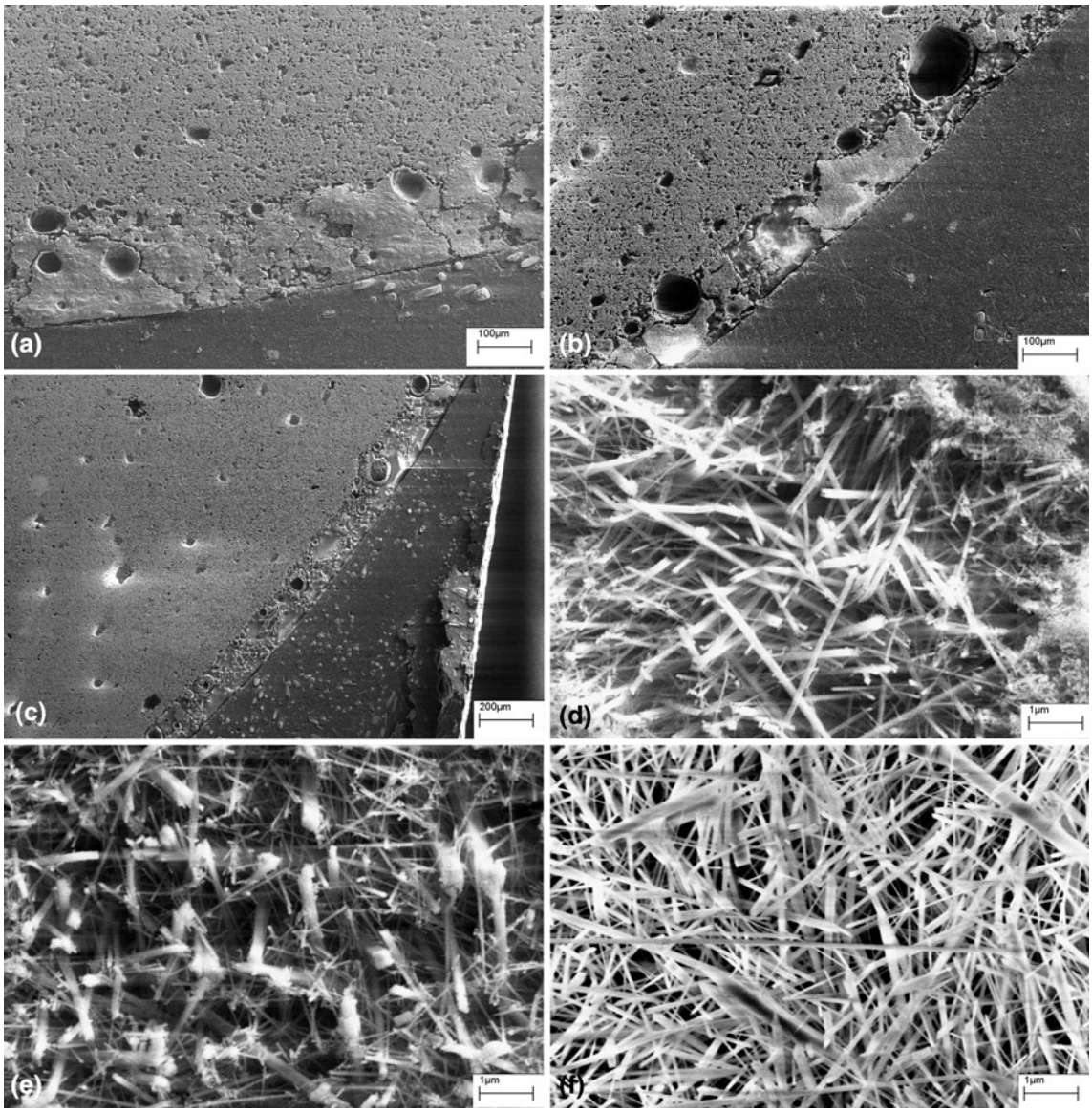

Fig. 10 Microstructure of glazed samples of (a) B, (b) D, and (c) E at low magnifications; and (d) B, (e) D, (f) E at high magnification. All samples were fired to 1250 °C and held at top temperature for 2 h, etched with 40% Hydrofluoric acid for 25 s. The higher magnification images are from the interior of the porcelain substrates

The high-magnification SEM micrographs in Fig. 10 reveal that the shape of mullite crystals in the interior of the three porcelain samples is quite similar. All samples exhibit long cylindrical mullite crystals. This is expected since the chemical compositions of their formulae are quite close.

4.6 Phase Constitution

X-ray diffraction analysis of powder samples of crushed glazed porcelains B, D, and E in Fig. 11 show identical XRD spectra. The crystalline phases in all samples are mullite and quartz as indicated in the figure.

4.7 Steger Tests

The Steger tests showed quite high values indicating that the glaze is in high compression. One value, +2.81 mm, was

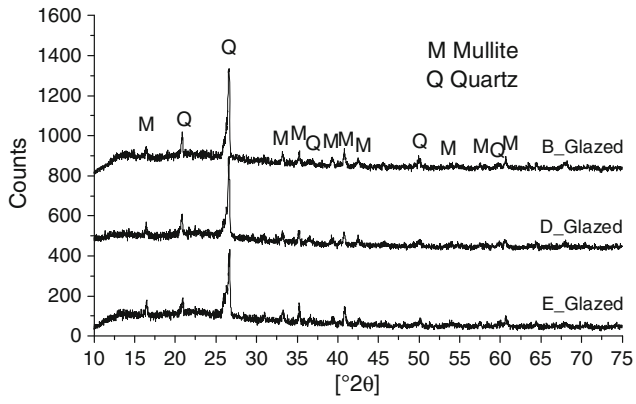

Fig. 11 XRD of powdered samples of glazed B, D, and E fired to 1250 °C and held at top temperature for 2 h

obtained for sample B and three values, +1.94, +2.15, and +2.04 mm, for sample E. These values are satisfactory according to the laboratory standard.

5. Discussion

The mixture of feldspar, clay, and sand, that forms porcelain continuously react with each other during heating. The three phases formed upon heating are glass, mullite, and quartz. The thermal expansion coefficient of each of the component phases produced upon firing are, respectively, 4-5.5 $\times 10^{-6}$, 5.3 $\times 10^{-6}$, and 15 $\times 10^{-6}$ °C^{-1} (Ref 15). Clearly quartz has the highest amount of expansion, hence influences the coefficient of thermal expansion depending on the amount present. Up to the quartz transition point, the biscuit-fired samples exhibit a very small change in length with temperature. The α-to-β quartz phase transition which occurs at ≈573 °C is accompanied by a volume change, which has been explained at a molecular level by the Rigid Unit Mode theory (Ref 16). This results in variation of the unit cell parameters with temperature leading to the β-quartz phase. The β-quartz phase, which exists at temperatures above 573 °C, has a negative thermal coefficient of expansion (Ref 16-18). The observed trend of negative coefficients of thermal expansion in the specimens is probably a result of the dominant effect of quartz in the samples.

Firing porcelain samples at higher temperatures leads to a reduction in the amount of crystalline quartz in the body due to its dissolution into the glassy phase. This lowers the magnitude of the thermal expansion coefficient of the resulting porcelain product. This explains the trend observed for sample E over the temperature range of 1100 to 1300 °C. Upon cooling, however, the β-quartz transforms back to α-quartz phase, as identified by x-ray diffraction.

All specimens showed an improvement in MOR upon glazing. This is a result of the contributory effects of phases formed and the interaction of the glaze with the bulk body. In relation to the thickness of the glaze layer, Kobayashi et al. (Ref 19) presented results suggesting that within the range of glaze thickness of 70-220 μm, strength of glazed specimens does not change considerably. Additionally, the bending strength is improved if the difference in thermal expansion between body and glaze is over 1.5 $\times 10^{-6}$ °C^{-1}. In this work, the glaze layer thickness is 120-170 μm suggesting that the same strengthening effect is expected. Indeed, the bending strength in all the glazed samples was improved but with varying levels of magnitude. It was high for sample B but small for sample E. The improvement is also partly due to the presence of a vitreous surface layer on the glazed samples, which covers any open surface cracks, thus sealing off fracture initiating flaws.

Differences in the coefficient of thermal expansion between body and glaze induces residual stress in glaze and body after cooling, and affects the mechanical strength of porcelain. Stresses in glaze and body after cooling can be calculated using Eq (2) and (3) (Ref 20).

$$\sigma_g = \frac{E_b \cdot E_g \cdot V \cdot \Delta\alpha \cdot \Delta T}{(1-\upsilon_b)\{E_b \cdot V + E_g(1-V)\}}, \quad \text{(Eq 2)}$$

$$\sigma_b = \frac{E_b \cdot E_g \cdot (1-V) \cdot \Delta\alpha \cdot \Delta T}{(1-\upsilon_b)\{E_b \cdot V + E_g(1-V)\}} \quad \text{(Eq 3)}$$

where, υ_b = Poisson's ratio of the body = 0.19 (Ref 21); E_b and E_g = Young's modulus of the body (75 GPa) and glaze (66.6 GPa), respectively, computed using expressions cited by Dumitrache et al. (Ref 22); V = Volume fraction of the body (taken as 0.9); $\Delta\alpha$ = Difference in thermal expansion of body and glaze; and ΔT = Difference in temperature of glass transition (taken as 750 °C) of glaze and room temperature (25 °C).

Using the above equations, computed compressive stresses of 71, 32, and 41 MPa are developed in the glaze layer on porcelains B, D, and E, respectively. The combination of glaze G3 with sample B results in high-compressive stresses within the glaze to cause the resultant increase in MOR registered in Fig. 6 compared to other samples. Steger test results on samples B and E support the positive effects of glaze G3 on sample B as compared to E.

As seen in Fig. 6, sintering for 2 h compared to sintering for 1 h results in a smaller slope, i.e., a lower Weibull's modulus. This can be explained as a reduction of flaws for the longer sintering time rendering more statistical uncertainty during mechanical testing. Upon glazing, on the other hand, the Weibull's modulus is increased and the lines are shifted toward higher stress. This means that the failure initiating flaws require higher stresses but have volume densities comparable to those existing after 1 h sintering.

The high K_{IC} exhibited by sample B also suggests that it has a high crystalline content and reduced porosity compared to the other samples. High crystallinity and reduced porosity in a ceramic body enhance mechanisms of crack tip shielding in which the load for fracture is transferred from the crack tip to other parts of the microstructure (Ref 23). This results in high MOR. The attained dielectric strength value of 18 kV/mm is above the minimum of 16 kV/mm cited by Richerson (Ref 24) for electrical porcelain, although falls short of the value of 25 kV/mm recommended by Moulson and Herbert (Ref 25), for high voltage insulation. The MOR value of 105 MPa obtained with glazed sample B compares well with values of 69 and 100 MPa cited by Richerson (Ref 24) and Moulson and Herbert (Ref 25), respectively, although these authors do not specify whether the values are for 3 or 4 point loading fixture.

Observation of the fractured specimens also revealed pores in the bulk samples D and E. This suggests that the firing schedule also affects the vitrification process of the studied porcelains differently. The interface bubbles observed between the glaze and the bulk ceramic body is reported to occur when the melting temperature of glaze is lower than the vitrification temperature of the bulk ceramic body due to gas expulsion during densification of the bulk ceramic. The gas in the bulk bodies, which is exhausted during densification, gets trapped between the melt glaze and sintered body. The trapped gas remains as bubbles inside the microstructure. These constitute points of weakness for crack growth during loading hence reducing strength. Although these bubbles have been revealed in the microstructures highlighted in the earlier paragraphs, the vitrification temperatures have not been investigated in this study.

6. Conclusion

Firing porcelain samples at a heating rate of 6 °C/mm to 1250 °C and soaking at the peak temperature for 2 h as

opposed to 1 h, improves both the mechanical and dielectric properties. A glaze with a Seger formula RO:0.57Al_2O_3:4.86-SiO_2 formulated from local materials was found to enhance the properties of a porcelain bulk body of 68% SiO_2, 19% Al_2O_3, and 4.7% K_2O. Application of the glaze on the porcelain bulk body improves the properties due to formation of a vitreous layer on the sample surfaces which reduces crack-initiating flaws. The contributory effect of glazing on porcelain strength is achieved when the difference in coefficients of thermal expansion between the bulk body and glaze results in greater compressive stresses in the glaze layer. This is in agreement with published literature. The sample, which showed the highest improvement in mechanical properties exhibited smooth rounded mullite needles in its microstructure. The values of MOR and K_{IC} attained with the best sample render it satisfactory for application in electrical insulation.

Acknowledgments

This work was funded by Sida/SAREC-Makerere University Collaborative Research Programme. The authors are grateful for the help from IFÖ Ceramics, Bromölla, Sweden in carrying out the Steger tests.

References

1. K. Bekir, M. Çaki, and S. Turan, The Development and Characterization of Zinc Crystal Glazes Used for Amakusa-like Soft Porcelains, *J. Eur. Ceram. Soc.*, 2000, **20**, p 2225–2231
2. A. Kara and R. Stevens, Interactions Between an ABS Type Leadless Glaze and a Biscuit Fired Bone China Body During Glost Firing. Part I: Preparation of Experimental Phases, *J. Eur. Ceram. Soc.*, 2002, **22**, p 1095–1102
3. M.G. Rasteiro, T. Gassman, R. Santos, and E. Antunes, Crystalline Phase Characterization of Glass-Ceramic Glazes, *Ceram. Int.*, 2007, **33**, p 345–354
4. M. Haberko and K. Haberko, Effect of Glaze on Strength of High Tension Porcelain, *Ceramurgia Int.*, 1975, **1**(1), p 28–32
5. R.A. Eppler and M. Obstler, *Understanding Glazes*, The American Ceramic Society, Ohio, USA, 2005, p 9–54
6. P.W. Olupot, S. Jonsson, and J.K. Byaruhanga, Development and Characterization of Triaxial Electrical Porcelains from Ugandan Ceramic Minerals, *Ceram. Int.*, in Press, Accepted Manuscript (Paper No. 613/2009)
7. P.W. Olupot, S. Jonsson, and J.K. Byaruhanga, Characterization of Feldspar and Quartz Raw Materials in Uganda for Manufacture of Electrical Porcelains, *J. Aust. Ceram. Soc.*, 2006, **42**(1), p 29–35
8. J.B. Kirabira, S. Jonsson, and J.K. Byaruhanga, Powder Characterization of High Temperature Ceramic Raw Materials in the Lake Victoria Region, *Silicate Ind.*, 2005, **70**(9–10), p 127–134
9. O.I. Ece and Z. Nakagawa, Bending Strength of Porcelains, *Ceram. Int.*, 2002, **28**, p 131–140
10. S.R. Bragança and C.P. Bergmann, A View of Whitewares Mechanical Strength and Microstructure, *Ceram. Int.*, 2003, **29**, p 801–806
11. G. Stathis, A. Ekonomakou, C.J. Stournaras, and C. Ftikos, Effect of Firing Conditions, Filler Grain Size and Quartz Content on Bending Strength and Physical Properties of Sanitary Ware Porcelain, *J. Eur. Ceram. Soc.*, 2004, **24**, p 2357–2366
12. H. Norsker and J. Danisch, *Glazes: For the Self-Reliant Potter*, Friedr. Vieweg & Sohn Verlagsgesellschaft mbH, Braunschweig, Germany, 1993, p 169
13. P.W. Olupot, S. Jonsson, and J.K. Byaruhanga, Effects of Mixing Proportions and Firing Temperature on Properties of Electric Porcelain from Ugandan Minerals, *Ind. Ceram.*, 2008, **28**(1), p 1–10
14. H. Baharav, B. Laufer, and R. Pilo, Effect of Glaze Thickness on the Fracture Toughness and Hardness of Alumina-Reinforced Porcelain, *J. Prosthet. Dent.*, 1999, **81**, p 515–519
15. A. Karamanov, E. Karamanova, A.M. Ferrari, F. Ferrante, and M. Pelino, The Effect of Fired Scrap Addition on the Sintering Behaviour of Hard Porcelain, *Ceram. Int.*, 2006, **32**, p 727–732
16. F.A. Gualtieri, Thermal Behaviour of the Raw Materials Forming Porcelain Stoneware Mixtures by Combined Optical and In Situ X-Ray Dilatometry, *J. Am. Ceram. Soc.*, 2007, **90**(4), p 1222–1231
17. T.H.K. Barron, J.F. Collins, T.W. Smith, and G.K. White, Thermal Expansion, Grüneisen Functions and Static Lattice Properties of Quartz, *J. Phys. C: Solid State Phys.*, 1982, **15**, p 3311–3326
18. M. Sternitzke and G. Müller, Crystal Structure and Thermal Expansion of Quartz-type Aluminosilicates, *J. Mater. Sci.*, 1991, **26**, p 3051–3056
19. Y. Kobayashi, O. Ohira, Y. Ohashi, and E. Kato, Effect of Glaze on Bending Strength of High Strength Whiteware Bodies, *J. Ceram. Soc. Jpn. Int. Ed.*, 1990, **98**(5), p 516–521
20. Y. Kobayashi, M. Mukai, T. Mizuno, O. Ohira, and H. Isoyama, Effect of Cristobalite Formation and Glaze on Bending Strength of α-Alumina Reinforced Porcelain, *J. Ceram. Soc. Jpn.*, 2005, **113**(6), p 413–418
21. J.A. Griggs, A. Kishen, and K.N. Le, Mechanism of Strength Increase for a Hydrothermal Porcelain, *Dent. Mater.*, 2003, **19**, p 625–631
22. R.L. Dumitrache, I. Teoreanu, and A. Valceanov, Limit Molecular Formulas and Target Formulas Determination for Feldspar Porcelain Glazes, *J. Eur. Ceram. Soc.*, 2007, **27**, p 1697–1701
23. S.M. Wiederhorn and E.R. Fuller Jr., Structural Behaviour of Ceramics, *Comprehensive Structural Integrity*, Vol. 2, I. Milne, R.O. Ritchie, and B.L. Karihaloo, Ed., Elsevier Science Ltd., 2002, p 1–26
24. D.W. Richerson, *Modern Ceramic Engineering: Properties, Processing, and Use in Design*, 2nd ed., Marcel Dekker, Inc., New York, 1992, p 162–312
25. A.J. Moulson and J.M. Herbert, *Electroceramics*, 2nd ed., John Wiley & Sons, England, 2003, p 269–273